applied sciences

MDPI

Article

Influence of Self-Compaction on the Airflow Resistance of Aerated Wheat Bulks (*Triticum aestivum* L., cv. 'Pionier')

Iris Ramaj *, Steffen Schock, Shkelqim Karaj and Joachim Müller

Tropics and Subtropics Group (440e), Institute of Agricultural Engineering, University of Hohenheim, 70599 Stuttgart, Germany

* Correspondence: i.ramaj@uni-hohenheim.de or info440e@uni-hohenheim.de; Tel.: +49-(0)-711-459-23119

Featured Application: Grain storage, design and analysis of cooling, aeration and low-temperature drying of in-store grain bulks, practical application.

Abstract: Aeration is a key post-harvest grain processing operation that forces air through the pore volume of the grain bulk to establish favorable conditions to maintain grain quality and improve its storability. However, during storage, grain bulk experiences self-compaction due to its dead weight, which alters the bulk properties and impedes the uniform flow of air during aeration. Thus, this study focused on investigating the effect of self-compaction on the pressure drop ΔP of wheat bulk (*Triticum aestivum* L., cv. 'Pionier', X = 0.123 kg·kg^{-1} d.b.) accommodated in a laboratory-scale bin (V_b = 0.62 m^3) at a coherent set of airflow velocities v_a. Pressure drop ΔP was measured at bulk depths H_b of 1.0, 2.0, 3.0 and 3.4 m and storage times t of 1, 65, 164 and 236 h. For the semi-empirical characterization of the relationship between ΔP and v_a, the model of Matthies and Petersen was used, which was proficient in describing the experimental data with decent accuracy (R^2 = 0.990, $RMSE$ = 68.67 Pa, $MAPE$ = 12.50%). A tailored product factor k was employed for the specific grain bulk conditions. Results revealed a reduction of in-situ pore volume ε from 0.413 to 0.391 at bulk depths H_b of 1.0 to 3.4 m after 1 h storage time t and from 0.391 to 0.370 after 236 h storage time t, respectively. A disproportional increase of the pressure drop ΔP with bulk depth H_b and storage time t was observed, which was ascribed to the irreversible spatio-temporal behavior of self-compaction. The variation of pore volume ε was modeled and facilitated the development of a generalized model for predicting the relationship between ΔP and v_a. The relative importance of modeling parameters was evaluated by a sensitivity analysis. In conclusion, self-compaction has proven to have a significant effect on airflow resistance, therefore it should be considered in the analysis and modeling of cooling, aeration and low-temperature drying of in-store grain bulks.

Keywords: aeration; airflow resistance; pore volume; semi-empirical modelling; self-compaction; spatial and temporal; wheat

Citation: Ramaj, I.; Schock, S.; Karaj, S.; Müller, J. Influence of Self-Compaction on the Airflow Resistance of Aerated Wheat Bulks (*Triticum aestivum* L., cv. 'Pionier'). *Appl. Sci.* **2022**, *12*, 8909. https://doi.org/10.3390/app12178909

Academic Editor: José Miguel Molina Martínez

Received: 9 August 2022
Accepted: 2 September 2022
Published: 5 September 2022

1. Introduction

Cereal grains are among the most important and indispensable food sources for humans, with an annual global production of 3.0 billion tons in 2020 [1]. They account for 60 to 80% of the dietary calorie intake, which makes up a significant portion of human energy and nutrient requirements [2]. Storage technologies play a critical role in maintaining the nutritional quality and prolonging the shelf-life of cereal grains during the off-season. Grain temperature and moisture content are the two most important parameters impacting storage, with high values affecting the intrinsic quality of grains and promoting decay [3–5]. The interaction between these parameters during storage has resulted in losses of about 13.4% in the global production in 2018 [6]. Therefore, aeration is utilized to force air through the pore volume of stored grain to modify the bulk microclimate and create favorable conditions for quality preservation and improvement of storability. Aeration

reduces the bulk temperature to a safe storage level to prevent insect and mite infestation, spontaneous heating and off-odors [7]. In addition, it inhibits the development of microflora by reducing the excess moisture and intergranular air humidity in isolated grain dump nests. Intergranular air humidity refers to the relative amount of water available in the air at a particular temperature described by sorption isotherms [8]. At sufficiently high levels (above 60%), the development of bacteria, fungi and yeasts is promoted, leading to the formation of toxins that are detrimental to humans [9,10]. Hence, ensuring adequate aeration throughout the grain bulk can be an important preservative measure to effectively control harmful substances.

During aeration, as the air flows through the pore volume of the grain bulk, it loses its kinetic energy due to intergranular friction and turbulence, resulting in airflow resistance known as pressure drop [11]. The grain species and cultivars, as well as their properties such as moisture content, physical and mechanical properties, surface roughness, bulk depth, pore volume configuration and extraneous impurity quantity, have a significant impact on the aeration process and uniformity of the airflow throughout the grain bulk [12–14]. They also influence the intergranular air pathways and associated inter-speed currents as well as the exchange of temperature and moisture in bulk [15]. Therefore, assessing the prevailing airflow resistance in grain bulks is essential for the energy-efficient design of ventilation systems, aeration management and grain quality retention [16].

Physical experiments are commonly used to assess the airflow resistance of grain bulks and serve as important means for the development of mathematical models. In this regard, Shedd [17] established an empirical model by fitting experimental data of pressure drop ΔP across the grain bulk and airflow velocity v_a for several grain types using a logarithmic scale. v_a referred to the hypothetical airflow velocity calculated from the volume flow rate in the free bulk cross-section area, also known as superficial velocity. However, Shedd's model was limited to a narrow range of airflow velocities, which was further enhanced by the model of Hukill and Ives [18]. Due to their ease of handling and simplicity, these models have been used in several studies [19–21]. In addition, Hunter [22] developed a lumped polynomial-based model capable of accurately anticipating the relationship of ΔP vs. v_a, but lacked insight into parameters affecting the airflow resistance. A modified version was proposed by Haque et al. [23] that included the moisture content as an input parameter. As these models were empirical in nature, they were tied to the same grain–air conditions and bin configurations for which they were created and therefore can outperform when those conditions vary widely.

To overcome the shortcomings of empirical models, semi-empirical models which use the grain's physical characteristics and air properties have been developed. Ergun [24] conducted a thorough data analysis to describe the relationship between ΔP and v_a of uniform spherical particles and developed a semi-empirical model based on the Kozeny-Carman [25] and Burke-Plummer relationships [26], making this model one of the most commonly analyzed and used in the literature. However, the Ergun model lacked adaptability to non-spherical shapes of particles, thus Patterson [27] and Li and Sokhansanj [28] suggested quantitative improvements to account for irregular and random-sized shapes of grains. A simplification of these models was proposed by Bern and Charity [29]. In addition, Leva [30] developed a semi-empirical model based on the Hagen-Poisseuille law for isothermal flow that contained a modified friction factor for the state-of-flow and a shape factor for non-spherical particles, while Matthies and Petersen [31] established another model for high grain bulks. Due to their theoretical underpinning, the semi-empirical models were able to determine the effect of different grains, moisture contents, filling methods, impurity concentration and airflow directions on the airflow resistance [12,13,23,32]. They were also viable in isolating and quantifying the grain bulk pore volume. A summary of the above-mentioned models for describing the relationship of ΔP vs. v_a in grain bulks is presented in Table 1. So far, the known models are limited to depicting the complexity and diversity of bulk pore structures [29].

Table 1. Models for describing the pressure drop ΔP as a function of airflow velocity v_a in grain bulks.

Source	Year	Model Type	Applicability		Comments
			Velocity v_a, $\mathbf{m \cdot s^{-1}}$	Type of Grains	
Ergun [24]	1952	Semi-empirical	≥0.01	Maize, rice, sorghum, wheat	Covers both laminar and turbulent flow; suitable for spherical particles
Shedd [17]	1953	Empirical	0.005–0.30	Barley, maize, oat, rice, sorghum, soybean, wheat	Appropriate for low airflow velocities and uncompacted grain bulk; outperformance at high velocities
Hukill and Ives [18]	1955	Empirical	0.0003–1.0	Barley, maize, oat, rice, sorghum, soybean, wheat	Encompasses a wide range of velocities; limited to specific grain and air conditions
Leva [30]	1959	Semi-empirical	≥0.0001	Barley, maize, oat, wheat	Tedious to solve; includes a friction-factor for the state-of-flow and a shape factor for non-spherical shape of grains
Patterson [27]	1969	Semi-empirical	0.05–0.61	Beans, maize	Adjusted model for grains with different size distributions and shape irregularities
Matthies and Petersen [31]	1974	Semi-empirical	0.02–0.61	Barley, maize, rice, rye, wheat	Established for high bulks; considers several influencing parameters
Bern and Charity [29]	1975	Semi-empirical	0.015–0.60	Maize	Easy to solve; considers solely pore volume and airflow velocity; limited to maize
Haque, Ahmed and Deyoe [23]	1982	Empirical	0.01–0.22	Maize, sorghum, wheat	Includes the effect of moisture content on the calculation basis
Hunter [22]	1983	Empirical	0.006–0.21	Barley, maize, oat, rice, sorghum, soybean, wheat	Better fit compared to Shedd; considers the non-uniform nature of grain bulks; lacks insight into parameters affecting airflow resistance
Li and Sokhansanj [28]	1992	Semi-empirical	0.0001–0.90	Barley, maize, oat, wheat	Similar to Ergun; suitable for grains; established for a wide range of airflow velocities

During storage, grain bulk undergoes burden pressures imposed by its dead weight, contributing to self-compaction [33–35]. Hence, the bulk characteristics may change depending on the degree of compaction. According to Rocha et al. [36], the airflow resistance in aeration systems is significantly increased with the increase of compaction when higher pressures are applied. Therefore, the misestimation of airflow resistance due to compaction can lead to ineffective aeration strategies and grain quality problems [35]. To date, the literature offers limited coverage on the effect of compaction on the airflow resistance of stored grain bulks where controlled compaction systems or filling methods were used [36–38]. However, the influence of spontaneous temporal and spatial self-compaction on the airflow resistance of practical storage systems has not been considered so far. Therefore, the objectives of this study were: (i) to investigate the effect of self-compaction on the pressure drop during aeration at various sets of airflow velocities, bulk depths and storage times, (ii) to mathematically describe the relationship of ΔP vs. v_a using a semi-empirical modeling

approach, (iii) to develop a generalized model with itemized product factor and variable bulk pore volume and (iv) to evaluate the influence of parameters in modeling of pressure drop through a sensitivity analysis.

2. Materials and Methods

2.1. Raw Material and Sample Preparation

A total quantity of 1000 kg wheat (*Triticum aestivum* L.), cultivar 'Pionier' (I.G. Pflanzenzucht GmbH, Ismaning, Germany) was obtained from the Heidfeldhof research farm of the University of Hohenheim, Stuttgart, Germany (48°42′56.54″ N, 9°11′23.07″ E). The non-cereal harvest impurities such as straw, chaff, dust and stones (8.86 ± 1.37%) of aggregate mass were removed using an automated cleaning machine (D-4950, Samatec Saatguttechnik & Maschinenbau GmbH, Bad Oeynhausen, Germany). The cleaned bulk was stored for 24 h at hygienically safe conditions (temperature T of 14.90 ± 1.50 °C and relative humidity φ of 52.09 ± 7.07%) before being used for measurement of physical properties and airflow resistance experiments.

2.2. Characterization of Grain Physical Properties

The moisture content X (kg·kg^{-1} d.b.) of wheat kernels was determined by the standard thermogravimetric analysis in a convective oven (UM 700, Memmert GmbH & CO. KG, Schwabach, Germany) at 105 ± 1 °C for 24 h and natural air circulation according to AOAC [39], where moisture of 0.123 ± 0.001 kg·kg^{-1} d.b. was observed (dry matter of 89.01 ± 0.01%).

The principal geometrical characteristics of kernels, length L (mm), width W (mm) and thickness T (mm) were measured via a digital Vernier caliper (Digi-Met IP 67, Helios-Preisser GmbH, Gammertingen, Germany) with a measuring resolution of ±0.01 mm. Measurements were carried out for a total of 100 randomly selected kernels. Shape-dependent geometric properties such as arithmetic diameter d_a (mm), geometric diameter d_g (mm), sphericity ϑ (%), aspect ratio R_a (-) and unit volume V (mm^3) were estimated from the basic geometrical characteristics, as described by Karaj and Müller [40]. The equivalent diameter d_e (mm) of kernels was calculated as:

$$d_e = \sqrt[3]{\frac{6\,V}{\pi}} \tag{1}$$

From Sirisomboon et al. [41], the surface area A (mm^2) of kernels was estimated as:

$$A = \frac{\pi\,W}{2}\left(W + \frac{L}{c}\arcsin c\right) \text{ with } c = \sqrt{1 - \left(\frac{W}{L}\right)^2} \tag{2}$$

In addition, the gravimetric properties were assessed. Unit mass m (g) of kernels was measured by means of an analytical high-precision balance with an accuracy of ±0.10 mg (Sartorius BP221S, Sartorius AG, Göttingen, Germany). Solid density ρ_s (kg·m^{-3}) was defined based on the toluene displacement method in a 25 mL pycnometer (Blaubrand, Wertheim, Germany) as described by Mohsenin [42]. Toluene was utilized as a water-insoluble liquid. The solid density ρ_s was determined as:

$$\rho_s = \frac{m_{gr}\,\rho_{tol}}{m_{gr} + m_{fl,\,tol} - m_{gr,\,fl,\,tol}} \tag{3}$$

where m_{gr} (g) is the mass of kernel, $m_{fl,tol}$ (g) is the mass of pycnometer flask filled with toluene, $m_{gr,fl,tol}$ (g) is the mass of kernels soaked in toluene solution together with the flask and ρ_{tol} (kg·m^{-3}) is the toluene density. The default bulk density ρ_{b0} (kg·m^{-3}) was measured by freely pouring kernels into a cylindrical container (150 mm diameter, 100 mm height) by maintaining a natural flow rate until overflowing. Afterwards, the surplus mass

was gently swiped off using a wooden striker from the brim of the container and weighted. Hence, the bulk density ρ_{b0} was calculated as:

$$\rho_{b0} = \frac{m_c}{V_c} \tag{4}$$

where m_c (kg) is amassed mass in the container and V_c (m^3) is the occupied volume. The default (uncompacted) pore volume ε_0 (-) was defined as the fraction of the volume of intergranular voids in the bulk and was calculated as a function of the solid density and bulk density:

$$\varepsilon_0 = 1 - \frac{\rho_{b0}}{\rho_s} \tag{5}$$

2.3. Experimental Test Bench

The test bench used to perform the airflow resistance experiments is shown schematically in Figure 1.

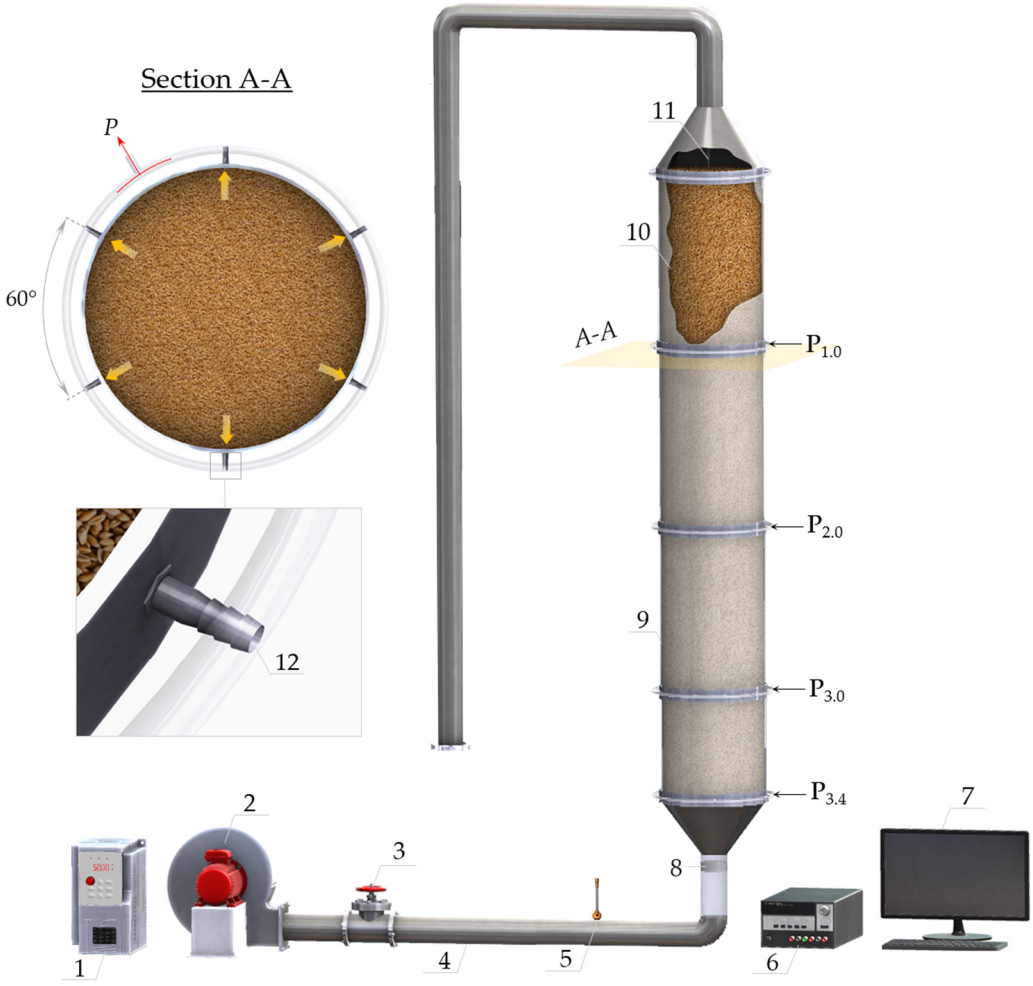

Figure 1. Test bench comprising (1) frequency inverter, (2) centrifugal fan, (3) safety valve, (4) air duct, (5) flow sensor, (6) data logger, (7) laboratory computer, (8) airflow straightener, (9) test bin, (10) wheat bulk, (11) sensor grid and (12) pressure taps. *P* denotes the equalized pressure of six pressure taps, whereas $P_{1.0}$, $P_{2.0}$, $P_{3.0}$ and $P_{3.4}$ represent the pressure data at bulk depths of 1.0, 2.0, 3.0 and 3.4 m, respectively.

A cylindrical acrylic-glass test bin (480 mm diameter, 3400 mm height and 5 mm wall thickness) with a wall friction coefficient of 0.32 ± 0.02 was used to accommodate approx. 500 kg of wheat kernels (V_b = 0.62 m^3). A perforated floor (3.80 mm apertures,

18.60% opening area) was installed at the bottom of the test bin to allow undisturbed upward movement of air within the pore volume of the grain bulk and to assert minimal resistance to airflow according to ASAE [43]. Air was supplied by a centrifugal fan (RD6-NRD80S/2, Elektror GmbH, Esslingen, Germany) with a maximal volumetric air capacity of 1230 $m^3 \cdot h^{-1}$, pressure of 2500 Pa at the nominal fan speed of 2890 min^{-1} and power consumption of 0.75 kW at 380 V/50 Hz. The fan speed was adjusted to the experimental requirements by a frequency inverter (ST 8100, Sourcetronic GmbH, Bremen, Germany).

An air duct (150 mm diameter, 2000 mm length) was employed to connect the fan with the test bin. A thermal flow sensor with an integrated transducer (TA10, Höntzsch Instrument, Waiblingen, Germany) with a measurement accuracy of ±2.0% was used to measure the airflow velocity at a distance of 10-fold diameter of the duct [44]. The flow sensor was calibrated using a bench wind tunnel (8390, TSI Incorporated, Shoreview, MN, USA). Based on the airflow velocity in the duct, the volume flow was calculated and subsequently the superficial velocity v_a in the test bin. At the duct end, a 90° bow rubber pipe and a honeycomb-shaped polycarbonate straightener (100 mm diameter, 50 mm thickness) were installed to prevent the fan propagating vibrations and ensure uniform flow conditions [12]. All joints of the test bench were examined for air leakage and were tightly sealed.

Pressure taps (2 mm diameter, 30 mm length) were attached in the wall of the test bin at depths of 1.0, 2.0, 3.0 and 3.4 m ($P_{1.0}$–$P_{3.4}$). The taps protruded 2 mm inside the bulk to reduce the possible wall effects during the pressure measurements. At each depth, six taps were evenly distributed around the circumference at a segment angle of 60° and connected by a loop of 4 mm diameter transparent polyethylene hose, which was also used to connect the loops with the pressure sensors (GMSD 25MR & GHM 3151-Ex, GHM Messtechnik GmbH, Remscheid, Germany) with an accuracy of ±0.50 Pa. Combined temperature/humidity sensors (SHT25, Sensirion AG, Zurich, Switzerland) were placed in the centerline of the test bin at the same depths as pressure sensors to measure the temperature T_a (±0.20 °C) and relative humidity φ_a (±1.80%) of intergranular air in the grain bulk. A data logger (Agilent 34901A, Agilent Technologies Inc., Santa Clara, CA, USA) was used to acquire data from all sensors and record them on a laboratory computer. Manual sampling and offline thermogravimetric analysis were also conducted to determine the grain moisture content in the bulk [39].

2.4. Experimental Procedure

A motor-driven screw conveyor (T206/4, Wolf Landtechnik GmbH, Petersberg, Germany) was used to fill the test bin and to ensure a practical filling procedure of grain bulk at a standard flow rate. The resulting bulk cone of approx. 30° was manually drawn off flush at the top edge [14]. After 1 h, during which the grain bulk rested, the fan was started with a frequency f of 10.0 Hz and gradually increased by 5.0 Hz intervals until 50.0 Hz, resulting in nine steps of airflow velocities. The fan speed was changed only when the fluctuations of the pressure readings were calming down to less than 2.0%. The pressure drop ΔP was estimated as the difference of pressure at H_b of 1.0 ($P_{1.0}$), 2.0 ($P_{2.0}$), 3.0 ($P_{3.0}$) and 3.4 m ($P_{3.4}$) to the pressure at the top of the test bin at H_b of 0.0 m bulk depth. In order to investigate the effect of self-compaction over time t, the same procedure was repeated after 65, 164 and 236 h. Table 2 shows the average fan speed ω, airflow velocity v_a, mass flow rate $\dot{m}$ and volume flow rate Q used for the experiments, which were chosen based on the practical recommendations for aeration and drying systems [45]. For the analysis of the relationship between pressure drop ΔP and airflow velocity v_a, a total of 15,760 data were gathered at different bulk depths H_b and storage times t. The intermittent forced aeration was applied only for the airflow resistance experiments, while the traditional storage without aeration was used for the rest of the time.

Table 2. Operating settings utilized for the airflow resistance experiments.

Frequency	Rotational Speed	Airflow Velocity	Mass Flow Rate	Volume Flow Rate
f, Hz	ω, min^{-1}	v_a, m·s^{-1}	$\dot{m}$, kg·h^{-1}	Q, m^3·h^{-1}
10.0	578	0.011 ± 0.000	8.57 ± 0.36	7.00 ± 0.29
15.0	867	0.021 ± 0.001	20.15 ± 0.96	16.46 ± 0.79
20.0	1156	0.037 ± 0.004	32.93 ± 3.40	26.90 ± 2.78
25.0	1445	0.056 ± 0.005	47.48 ± 4.25	38.79 ± 3.47
30.0	1734	0.074 ± 0.006	61.37 ± 4.66	50.14 ± 3.81
35.0	2023	0.092 ± 0.006	74.99 ± 5.04	61.27 ± 4.12
40.0	2312	0.109 ± 0.008	88.14 ± 6.28	72.01 ± 5.14
45.0	2601	0.125 ± 0.008	100.78 ± 6.61	82.34 ± 5.40
50.0	2890	0.141 ± 0.010	113.16 ± 8.37	92.45 ± 6.84

2.5. Semi-Empirical Modelling of Airflow Resistance

Out of the available semi-empirical models in literature, the Matthies and Petersen [31] was chosen as the most appropriate for modeling ΔP vs. v_a of grain bulks $H_b \geq 2.50$ m, which covers the irregular and random-sized shapes of wheat kernels and a wide range of airflow velocities. This model is expressed as:

$$\frac{\Delta P}{H_b} = k\,\zeta\,\frac{\rho_a\,{v_a}^2}{2\,d_e\,\varepsilon^4} \tag{6}$$

where ΔP (Pa) is the pressure drop in bulk, v_a (m·s^{-1}) is the airflow velocity, H_b (m) is the bulk depth, k (-) is the product factor related to the shape configuration, size and surface characteristic of wheat kernels, ζ (-) is the coefficient of air resistance, ρ_a (kg·m^{-3}) is the density of intergranular air and ε (-) is the pore volume of grain bulk. The product factor k was estimated by fitting the model to the experimental data, while the coefficient of air resistance ζ was determined as:

$$\zeta = \frac{47.92}{Re} + \left(\frac{1.18}{Re}\right)^{0.1} \tag{7}$$

where Re (-) is the Reynolds number, which was expressed as a function of the equivalent diameter of kernels d_e (mm):

$$Re = \frac{v_a\,\rho_a\,d_e}{\mu_a} \tag{8}$$

where μ_a (kg·m^{-1}·s^{-1}) is the dynamic viscosity of air in the pore volume of grain bulk. The thermodynamic characteristics of air μ_a, ρ_a and Reynolds number Re were calculated based on the temperature T_a and relative humidity φ_a of intergranular air of grain bulk during aeration. Therefore, the Matthies and Petersen [31] model (Equation (6)), by embedding the Re and ζ, can be written as:

$$\frac{\Delta P}{H_b} = k\left(\frac{23.96\,\mu_a v_a}{\varepsilon^4 d_e^2} + \frac{0.51\,\mu_a^{0.1}\rho_a^{0.9}{v_a}^{1.9}}{\varepsilon^4 d_e^{1.1}}\right) \tag{9}$$

The above-mentioned equation was used to fit the experimental data of ΔP vs. v_a at various bulk depths and storage times.

2.6. Statistical Analysis and Graphical Presentation

The graphical representation of data and the nonlinear least-squares fitting procedure at 95.0% significance level ($p \leq 0.05$) were carried out in MATLAB 2019a (MathWorks Inc., Natick, MA, USA). The Levenberg-Marquardt algorithm was used for the fitting of experimental data in a series of iterative steps with a convergence criterion of 1.0×10^{-6}. The coefficient of determination R^2, root mean square error $RMSE$ and mean absolute

percentage error *MAPE* were employed as statistical criteria to assess the goodness of fit, which were defined as follows:

$$R^2 = 1 - \frac{\sum_{i=1}^{n}\left(\Delta P_{obs} - \Delta P_{pred}\right)^2}{\sum_{i=1}^{n}\left(\Delta P_{obs} - \overline{\Delta P_{obs}}\right)^2} \quad (10)$$

$$RMSE = \sqrt{\frac{\sum_{i=1}^{n}\left(\Delta P_{obs} - \Delta P_{pred}\right)^2}{n}} \quad (11)$$

$$MAPE = \frac{100}{n}\sum_{i=1}^{n}\left|\frac{\Delta P_{obs} - \Delta P_{pred}}{\Delta P_{obs}}\right| \quad (12)$$

where ΔP_{pred} (Pa) is the predicted pressure drop, ΔP_{obs} (Pa) is the observed pressure drop ascertained from experiments and n (-) is the number of observations. The sensitivity analysis using Monte Carlo simulations in MATLAB/Simulink 2019a (MathWorks Inc., Natick, MA, USA) performed to evaluate the influence of modeling parameters on pressure drop. Furthermore, the CAD design of the experimental test bench was carried out in SOLIDWORKS 2019 (Dassault Systèmes, Waltham, MA, USA).

3. Results and Discussion

3.1. Characterization of Grain Physical Properties

Table 3 presents the summary of the geometric and gravimetric properties of wheat kernels (*Triticum aestivum* L.) cv. 'Pionier' at moisture content of 0.123 ± 0.001 kg·kg^{-1} d.b.

Table 3. Geometric and gravimetric properties of wheat (*Triticum aestivum* L.) cv. 'Pionier'.

Properties	Unit	Value
Length L	mm	6.87 ± 0.25
Width W	mm	3.75 ± 0.22
Thickness T	mm	3.11 ± 0.17
Arithmetic diameter d_a	mm	4.57 ± 0.15
Geometric diameter d_g	mm	4.30 ± 0.15
Equivalent diameter d_e	mm	4.49 ± 0.14
Aspect ratio R_a	-	0.55 ± 0.03
Sphericity ϑ	%	62.72 ± 1.94
Surface area A	mm^2	64.06 ± 5.42
Volume V	mm^3	41.95 ± 4.34
Unit mass m	g	0.06 ± 0.01
Bulk density ρ_{b0}	kg·m^{-3}	782.46 ± 6.68
Solid density ρ_s	kg·m^{-3}	1351.40 ± 4.62
Pore volume ε_0	-	0.421 ± 0.07

It can be discerned from Table 3 that a low standard deviation was exhibited from geometric properties, indicating that data were tightly clustered around the mean value. The length L, width W and thickness T were found to be consistent with the literature, with values falling within 5.78–7.45 mm, 2.36–3.93 mm, 2.56–3.27 mm reported by Tabatabaeefar [46], Karimi et al. [47], Molenda and Horabik [48] and Wang et al. [49] for other wheat varieties but similar moisture contents. Therefore, the shape-dependent properties such as arithmetic diameter d_a, geometric diameter d_g, equivalent diameter d_e, aspect ratio R_a, sphericity ϑ, surface area A and unit volume V were also in conformity with the same literature. However, kernel dimensions were slightly larger than those reported by Giner and Denisienia [12], Nelson [50], Petingco et al. [51] and Markowski et al. [52], which can be attributed to differences in sample origin, cultivar, specific growth conditions and moisture contents. Gürsoy and Güzel [53], on the other hand, reported lower values for width and thickness for similar kernel lengths, resulting in a lower aspect ratio R_a and sphericity ϑ.

In addition, the gravimetric properties are presented in Table 3. Due to the larger kernel dimensions, a larger unit mass m was observed compared to values reported by Gürsoy and Güzel [53] and Markowski, Żuk-Gołaszewska and Kwiatkowski [52]. The values of bulk density ρ_{b0}, solid density ρ_s and pore volume ε_0 were found to be in decent agreement with values reported by Molenda and Horabik [48], Haque et al. [23], Jayas and Cenkowski [54], Muir and Sinha [55] and Kraszewski [56]. However, higher values of bulk density ρ_{b0} and pore volume ε_0 were observed compared to Markowski, Żuk-Gołaszewska and Kwiatkowski [52], which can be ascribed to the cultivar and/or kernel moisture content, as well as container volume, size, quantity of impurities, filling procedure and filling height and rate, which in turn affected the bulk packing in the container [57,58]. In contrast to Giner and Denisienia [12], lower values of bulk density ρ_{b0} were obtained, resulting in a higher pore volume ε_0 for similar solid density ρ_s.

3.2. Bulk Conditions during Experimentation

During pressure drop experiments, variations in temperature T_a from 12.29 to 17.18 °C and relative humidity φ_a from 34.04 to 40.87% were observed for the intergranular air of the grain bulk at 1, 65, 164 and 236 h storage time t. The associated thermodynamic properties of air, in terms of viscosity μ_a and density ρ_a, were assessed according to White and Majdalani [59] and tabulated in Appendix A (Table A1). The observed data were utilized for the semi-empirical modeling of pressure drop. Despite fluctuations in temperature T_a and relative humidity φ_a, no significant differences were observed in moisture content X of the wheat bulk (0.123 ± 0.001 to 0.122 ± 0.001 kg·kg^{-1} d.b.) at $p \leq 0.05$ during the experiments, which means that possible effects of drying on the self-compaction were excluded.

3.3. Determination of the Product Factor k

Matthies and Petersen [31] found a product factor k ranging from 2.00 to 2.20 in their study for calculating the airflow resistance of stored wheat bulks. However, a different wheat variety with different moisture content, physical properties, kernel size distribution and filling method has been employed in this study, therefore the value of k was tailored to the specific grain bulk and experimental conditions. Herewith for the determination of k, the experimental data of ΔP vs. v_a for bulk depths of H_b 1.0, 2.0, 3.0 and 3.4 m and storage time t of 1 h were fitted by the Matthies and Petersen model (Equation (9)) and the pore volume ε at different depths H_b was determined, accordingly. The observed ε were afterwards fitted by a linear model to describe the relationship between ε and H_b and extrapolated to H_b = 0.1 m, which is the criterion for comparison with the default ε_0 (uncompacted) ascertained in the laboratory. First, the reported k were used and afterwards k was iteratively adjusted by intervals of 0.01 until the predicted pore volume matched the default ε_0 of 0.421 (Figure 2). By using this criterion, a value of k of 2.73 was found, which fell between values of 2.00 and 3.90 used for various grains by Matthies and Petersen [31]. This finding was consistent with findings of Bakker-Arkema et al. [60] and Patterson [27], who adjusted the factor k for the specific settings of their experiment and found out higher values of k than those reported by Matthies and Petersen [31].

The linear models and the goodness of fit acquired from individual fittings at k of 2.00, 2,10, 2.20 and 2.73 are presented in Table 4. An accuracy of $R^2 \geq 0.985$ was observed from fitting with the linear models, which indicated a high capability of the employed models to depict the relationship between ε and H_b at different k. Figure 2 displays graphically the variation of the pore volume ε influenced by factor k with respect to the default ε_0. It can be seen that the values of ε increased proportionally with the increase of k. The values proposed by Matthies and Petersen [31] resulted in underestimation of 7.31, 6.17 and 5.09% of default ε at H_b = 0.1 m for k of 2.00, 2.10 and 2.20, respectively. Moreover, these factor k yielded a *MAPE* of 26.82, 23.17 and 19.51% for pressure drop in fitting the experimental data. Therefore, a product factor k of 2.73 was used for prediction of pressure drop of wheat bulk cv. 'Pionier'.

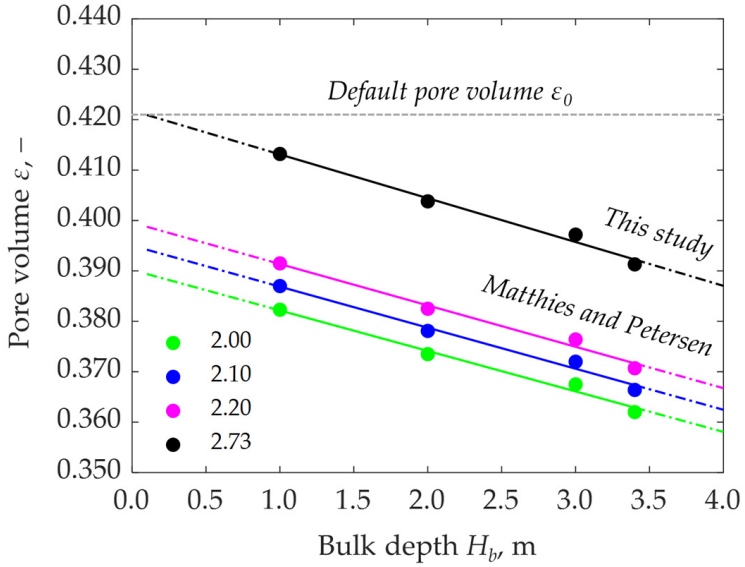

Figure 2. Pore volume ε vs. bulk depth H_b for product factor k of 2.00, 2.10, 2.20 and 2.73. Horizontal dashed line refers to the default pore volume ε_0 at bulk depth H_b of 0.1 m. Solid lines represent linear model fitting; dashed lines represent extrapolations beyond the dataset utilized for fitting.

Table 4. Linear models for describing the relationship between the pore volume ε and bulk depth H_b at different product factor k and coefficient of determination R^2.

Product Factor k, -	Mathematical Model	R^2, -
2.00	$y = -8.027 \times 10^{-3}\, x + 0.390$	0.986
2.10	$y = -8.141 \times 10^{-3}\, x + 0.395$	0.986
2.20	$y = -8.215 \times 10^{-3}\, x + 0.400$	0.985
2.73	$y = -8.693 \times 10^{-3}\, x + 0.422$	0.986

3.4. Influence of Self-Compaction on the Airflow Resistance

Figure 3a shows the experimental data of the pressure drop ΔP vs. airflow velocity v_a at bulk depths H_b of 1.0, 2.0, 3.0 and 3.4 m at 1 h storage time t. The overall variation of ΔP during the measurement cycle was relatively small, with the standard deviation ranging from 0.51 to 24.86 Pa, which indicated that the data were highly reproducible and tightly clustered around the mean values. The experimental data exhibited a progressive increase in pressure drop ΔP with increasing air velocity v_a and bed depth H_b, which were comparable to those of Giner and Denisienia [12] for similar moisture content and velocities smaller than 0.15 m·s^{-1}. This can be explained by the application of the same filling procedure that produced a dense bulk configuration as is typically used in practice. A similar trend of pressure drop for wheat was reported by Molenda et al. [37] for sprinkle filling. However, the results of ΔP vs. v_a were higher than those of Shedd [17] and Haque et al. [23], which can be attributed to the differences in wheat varieties and filling methods, resulting in higher resistance to airflow and higher pressure drops.

When fitting the Matthies and Petersen [31] to the experimental data and using the default pore volume ε_0 of 0.421 as obtained from laboratory measurements, where the curves were found to increasingly deviate with increasing airflow velocity v_a and bulk depth H_b. For H_b = 1.0 m, a decent fit is observed for $v_a \leq 0.10$ ms^{-1}, after which the model tends to underestimate the experimental data values by up to 11.78%. Notably, this tendency becomes more prominent with the increase of H_b to 2.0, 3.0 and 3.4 m, where differences increase with a deviation up to 19.62, 24.61 and 28.92%, respectively. Hence, the observed results were found to be irreconcilable with the homogeneous and isotropic consideration of grain bulk reported in literature, for which the pressure drop curves between depths H_b are linearly equidistant at a given velocity v_a, as the curves from

prediction underestimated the behavior of the experimental data. Figure 3b shows the distribution of predicted ΔP_{pred} vs. observed ΔP_{obs} for the default pore volume ε_0.

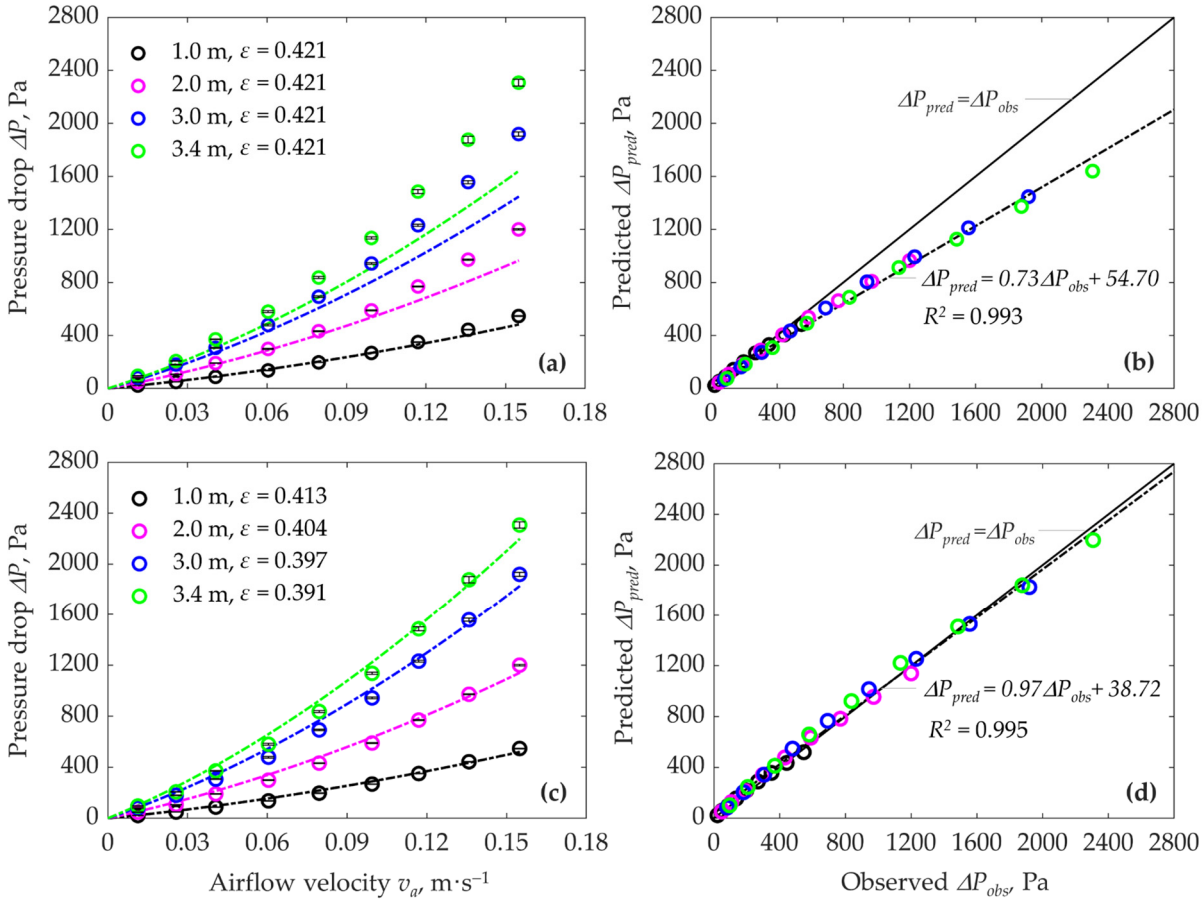

Figure 3. Experimental and predicted pressure drop ΔP vs. airflow velocity v_a at bulk depth H_b of 1.0, 2.0, 3.0 and 3.4 m and storage time t of 1 h storage time fitted with (**a**) default pore volume ε_0 of 0.421 and (**c**) adjusted pore volume ε between 0.391 and 0.413. Markers represent the experimental data points (±SD), dashed-dotted lines indicate fitting with the Matthies and Petersen model; Predicted pressure drop ΔP_{pred} vs. observed pressure drop ΔP_{obs} for (**b**) default and (**d**) variable pore volume.

It can be seen that the model exhibit an inferior performance with the data deviating from $\Delta P_{pred} = \Delta P_{obs}$ line and clustering towards the line $\Delta P_{pred} = 0.73\Delta P_{obs} + 54.70$ with $R^2 = 0.993$ and thus revealing an average underestimation of 22.0%. This disparity, however, is likely to increase as velocity v_a exceeds the limit used in this study.

To account for the spatial change of the pore volume in the grain bulk caused by self-compaction, the experimental data were refitted for each bulk depth H_b by adjusting the ε values. A reduction in pore volume ε of 0.413, 0.404, 0.397 and 0.391 was found from fitting analysis for H_b of 1.0, 2.0, 3.0 and 3.4 m. The variation of the pressure drop ΔP using the variable pore volumes ε is displayed in Figure 3c, where the fitted curves have accurately described the course of the experimental data. When using adjusted pore volume ε, the distribution of data was closely dispersed around the line $\Delta P_{pred} = 0.97\Delta P_{obs} + 38.72$ in close proximity with line $\Delta P_{pred} = \Delta P_{obs}$, hence revealing a high accuracy prediction with $R^2 = 0.995$ by the employed model (Figure 3d). These results were accredited to the vertical decrease of pore volume ε by 5.30%, which was in line with the findings of Cheng et al. [61] for compressive pressure levels ranging from 0 to 50 kPa. This behavior can be explained by the pressure of the overlying grain mass, which increases the in-situ intergranular stresses between kernels due to the dead weight of the overlying bulk [33]. Consequently, the pressure drop ΔP increased non-uniformly with the increase of the bulk depth H_b.

Since self-compaction is a dynamic process, the ΔP vs. v_a were fitted for different storage times t and the pore volume ε was also adjusted. Results of ε for bulk depths H_b of 1.0, 2.0, 3.0 and 3.4 m and storage time t of 1, 65, 164 and 236 h are shown in Figure 4. The default pore volume ε_0 was indicated by the grey plane in the chart.

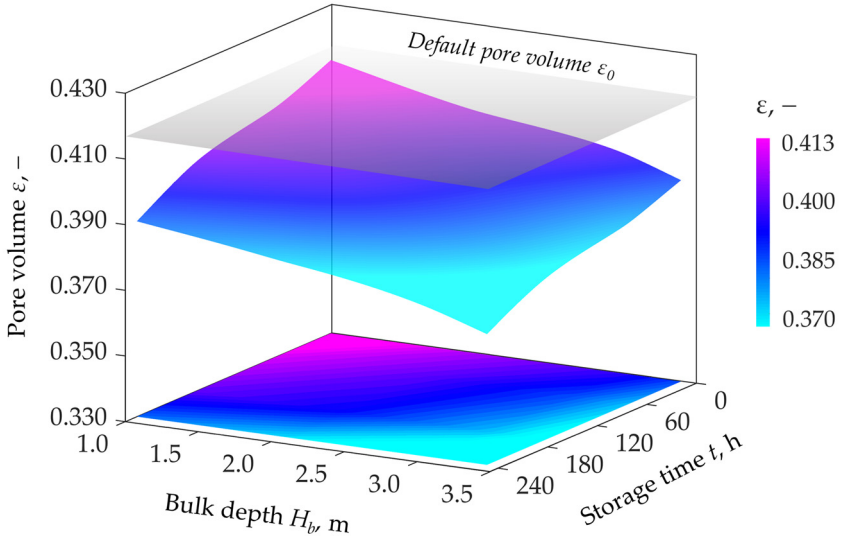

Figure 4. Variation of pore volume ε with bulk depth H_b and storage time t. The grey plane indicates the default pore volume ε_0.

For the different bulk depths H_b of 1.0 to 3.4 m, a temporal decrease of ε from 0.413 to 0.391, from 0.406 to 0.385, from 0.400 to 0.379 and from 0.390 to 0.370 was observed when storage time t increased from 1 to 65, 164 and 236 h. The resultant stresses are believed to initially influence the reorientation of the kernels and then cause the irreversible plastic deformation once the rupture force is attained, which eventually decreases the pore volume ε [33]. The compaction of the grain mass can be attributed to the visco-elastoplastic properties of kernels. However, Figure 4 shows that the grain mass did not settle completely and a longer time can be required to achieve the permanent equilibrium.

Figure 5 presents the pressure drop ΔP vs. airflow velocity v_a for storage time t predicted with the Matthies and Petersen model. It can be seen that the pressure drop manifested a temporal increase throughout 236 h of storage time t, which can be ascribed to the gradual and irreversible dynamic compaction of the bulk [62,63]. Hence, a variation of pressure drop ΔP from 1231.92 to 1536.97 Pa was estimated for 3.40 m bulk depth H_b at v_a = 0.10 m·s^{-1} once the storage time t increased from 1 to 236 h, which accounted for an increase of 24.76%. The higher pressure drops are mainly attributed to the dense fill created by the kernel packing due to the reduction of pore volume ε, which leads to increased kinetic energy dissipation due to friction and turbulence and higher intergranular resistances of the airflow. Similar outcomes were reported by Kumar and Muir [32], Molenda et al. [37] and Łukaszuk et al. [38], who found a considerable increase in pressure drop ΔP due to increase of ρ_b and reduction of ε obtained from the application of different filling methods and filling height. The same tendency has been also noted by Jayas et al. [64] for rapeseed, Kay et al. [65] for maize and Siebenmorgen and Jindal [66] for rice. However, they used the mean pore volume ε for modeling the relationship between ΔP and v_a and did not encounter the lateral variation of ε caused by self-compaction. Moreover, the results of this study are consistent with the outcomes of Haque [67], who confirmed the effect of non-homogeneous bulk of wheat on the pressure drop per unit of bulk depth due to self-compaction. Khatchatourian and Savicki [68] reported similar findings for soybeans. Despite consistency with published research, the effect of storage time t on ΔP has not been reported so far.

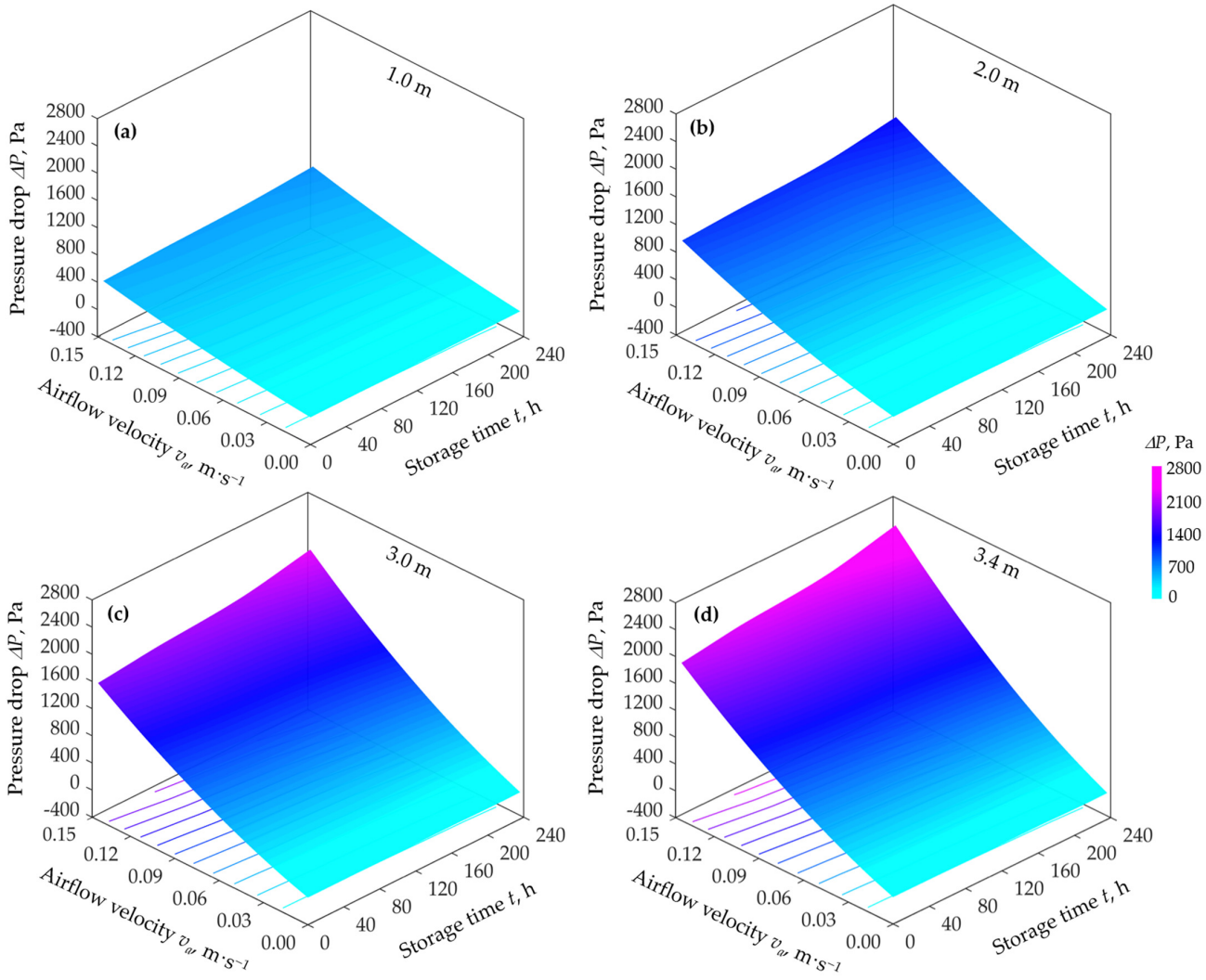

Figure 5. Pressure drop ΔP vs. airflow velocity v_a and storage time t predicted with the Matthies and Petersen model at bulk depths H_b of 1.0, 2.0, 3.0, 3.4 m (**a**–**d**).

A summary of adjusted pore volumes ε and statistical indicators attained from the fitting analysis is given in Table 5. The inspection of the statistical indicators revealed that the Matthies and Petersen [31] model was capable of depicting the course of ΔP vs. v_a at a decent accuracy. Particularly, R^2 between 0.983 and 0.996, *RMSE* between 15.18 and 123.77 Pa and *MAPE* between 8.21 and 16.16% were observed, respectively. However, a slight overestimation was observed at all predicted curves from 0.06 to 0.09 m·s^{-1}. Furthermore, from Table 5 can be discerned an increase in bulk density ρ_b which goes along with the decrease of pore volume ε. Particularly, a variation of 793.00–822.60 kg·m^{-3}, 802.33–830.98 kg·m^{-3}, 810.98–938.95 kg·m^{-3} and 825.03–851.65 kg·m^{-3} was observed for the bulk density ρ_b at the bulk depths H_b of 1.0 to 3.4 m and storage times t of 1, 65, 164, 236 h, respectively.

Figure 6a presents the data from pooling all predicted ΔP_{pred} and experimental ΔP_{obs} from the fitting analysis. It can be seen that the experimental data were satisfactorily anticipated by the model since they fell around the line of $\Delta P_{pred} = \Delta P_{obs}$, hence showing an appropriate accuracy of prediction of the Matthies and Pettersen model for the employed range of v_a, H_b and t with an $R^2 = 0.990$, *RMSE* = 68.67 Pa, *MAPE* = 12.50%.

Table 5. Pore volume ε and bulk density ρ_b for different storage time t and bulk depth H_b as well as statistical indicators (R^2, *RMSE*, *MAPE*) observed from fitting the experimental data with Matthies and Peterson model.

Storage Time t, h	Bulk Depth H_b, m	Pore Volume ε, -	Bulk Density ρ_b, kg·m^{-3}	Statistical Indicators		
				R^2, -	*RMSE*, Pa	*MAPE*, %
1.0	1.0	0.413	793.00	0.995	15.18	8.21
	2.0	0.404	805.70	0.995	33.28	8.32
	3.0	0.397	814.62	0.995	52.39	7.19
	3.4	0.391	822.60	0.996	61.93	7.62
65.0	1.0	0.406	802.33	0.983	29.19	14.75
	2.0	0.400	811.38	0.983	62.74	15.12
	3.0	0.391	822.46	0.983	100.65	14.40
	3.4	0.385	830.98	0.982	123.77	13.97
164.0	1.0	0.400	810.98	0.987	26.58	16.16
	2.0	0.395	817.73	0.987	54.16	14.44
	3.0	0.385	831.11	0.987	89.30	13.28
	3.4	0.379	838.95	0.987	106.91	13.66
236.0	1.0	0.390	825.03	0.993	21.04	14.61
	2.0	0.383	833.27	0.993	45.24	15.11
	3.0	0.375	844.08	0.993	68.35	10.66
	3.4	0.370	851.65	0.993	84.17	12.75

The frequency distribution of residuals is shown in Figure 6b. The results indicate that the residuals follow a random distribution. This distribution was found to be unbiased and homoscedastic with non-constant variance, hence a reasonably symmetric and unimodal distribution of residuals around 0 was observed, which supported the validity of the engaged model. The values of residuals ranged from −169.24 to 233.55. However, 55.0% of data fell between −34.97 and 9.78. According to the Shapiro-Wilk test, the residuals indicated a significant likelihood of non-normal distribution at $p \leq 0.05$. Hence, a logistic model was employed to describe the distribution behavior of residuals.

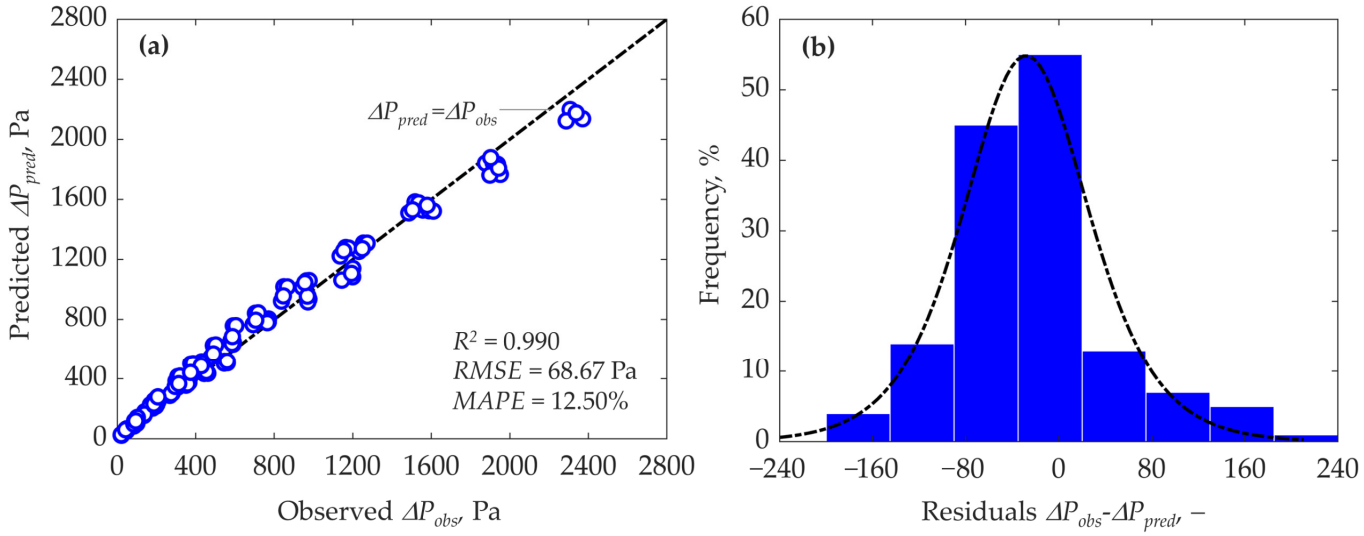

Figure 6. (**a**) Predicted pressure drop ΔP_{pred} vs. observed pressure drop ΔP_{obs} from pooled data of bulk depth H_b of 1.0, 2.0, 3.0, 3.4 m and storage times t of 1, 65, 164, 236 h; (**b**) Frequency distribution of residuals. Dashed-dotted line indicates the logistic probability distribution of residuals.

3.5. Modelling of Pore Volume Variation in Bulk

To establish a generalized semi-empirical model, pore volume ε was expressed as a function of bulk depth H_b analogous to the model proposed by Gao et al. [69] and Cheng et al. [35] for bulk density, which is given as:

$$1 - \frac{\varepsilon_0 - \varepsilon}{\varepsilon_0 - \varepsilon_{min}} = aH_b + c \tag{13}$$

where ε_0 (-) refers to the default pore volume and ε_{min} (-) refers to the minimal pore volume observed at the highest bulk depth H_b of 3.4 m, while a and c are the empirical constants observed from fitting analysis. To determine the pore volume ε, Equation (13) was rewritten as:

$$\varepsilon = \varepsilon_0 - (\varepsilon_0 - \varepsilon_{min}) \cdot (1 - aH_b - c) \tag{14}$$

Table 6 presents the equations and goodness of fit derived from the regression analysis for the different storage times t. The constants a and c were embodied in the equations. A variation of constant a from -0.292 to -0.156 and c from -1.026 to -0.557 was observed accordingly, hence revealing a decreasing trend of constants a and c with the increase of storage time t. The statistical indicators confirmed the capability of the employed model to predict closely the data with a high accuracy of $R^2 \geq 0.963$.

Table 6. Mathematical models for describing pore volume ε as function of bulk height H_b at different storage times t.

Storage Time t, h	Mathematical Model	R^2, -
1	$\varepsilon = \varepsilon_0 - (\varepsilon_0 - \varepsilon_{min}) \cdot (1 + 0.292H_b - 1.026)$	0.987
65	$\varepsilon = \varepsilon_0 - (\varepsilon_0 - \varepsilon_{min}) \cdot (1 + 0.238H_b - 0.851)$	0.977
164	$\varepsilon = \varepsilon_0 - (\varepsilon_0 - \varepsilon_{min}) \cdot (1 + 0.205H_b - 0.733)$	0.963
236	$\varepsilon = \varepsilon_0 - (\varepsilon_0 - \varepsilon_{min}) \cdot (1 + 0.156H_b - 0.557)$	0.980

In analogy with Equation (14), a model for describing pore volume ε as function of bulk height H_b and storage time t with an R^2 of 0.972 could be established:

$$\varepsilon = \varepsilon_0 - (\varepsilon_0 - \varepsilon_{min}) \cdot (1 + 0.016H_b + 0.002t - 1.013) \tag{15}$$

This allowed the inclusion of the influence of bulk depth H_b and storage time t in the Matthies and Petersen model (Equation (9)), hence yielding a generalized model:

$$\Delta P = 2.73 \cdot \left(\frac{23.96\ \mu_a v_a}{d_e^2} + \frac{0.51\ \mu_a^{0.1} \rho_a^{0.9} {v_a}^{1.9}}{d_e^{1.1}} \right) \cdot \left(\frac{H_b}{(\varepsilon_0 - (\varepsilon_0 - \varepsilon_{min}) \cdot (1 + 0.016H_b + 0.002t - 1.013))^4} \right) \tag{16}$$

The generalized model was able to depict the airflow resistance of wheat with an R^2 of 0.989, *RMSE* of 75.91 Pa and *MAPE* of 16.29%.

3.6. Sensitivity Analysis

The relative importance of parameters in modeling of pressure drop ΔP was determined through a sensitivity analysis, which was performed by generating a randomized combination of input parameters (v_a, H_b, ε, d_e, ρ_a, μ_a) of Equation (9) within their range of operating conditions and evaluating their impact on pressure drop ΔP. Figure 7 presents the standardized regression coefficients of sensitivity analysis, with parameters ranked by influence. Results of the analysis indicated that air velocity v_a is the most influential parameter, which significantly influences the pressure drop ΔP due to its contribution to energy dissipation of air pathways due to friction and turbulence. A value of 0.85 was obtained, indicating how decisive v_a is for the airflow resistance and aeration process of wheat bulk. Therefore, bulk depth H_b makes a considerable contribution in ΔP, where a value of 0.47 was observed, demonstrating a relatively weaker influence (-44.71%) compared to

airflow velocity v_a. Noticeably, v_a and H_b are positively correlated with ΔP, therefore higher values of velocity or bulk depth result in the increase of pressure drop with the magnitude determined by the analysis. Pore volume ε and particle diameter d_e were identified as less decisive, which negatively affect ΔP with values of -0.18 and -0.15, respectively. They are responsible for the bulk configuration, therefore, their reduction increases the resistance to airflow and consequently increases the pressure drop ΔP. The parameters that had the least influence were air density ρ_a (0.05) and dynamic viscosity of air μ_a (0.01) which were affected by the minor variations of temperature T_a and relative humidity φ_a of the air passing through the grain bulk.

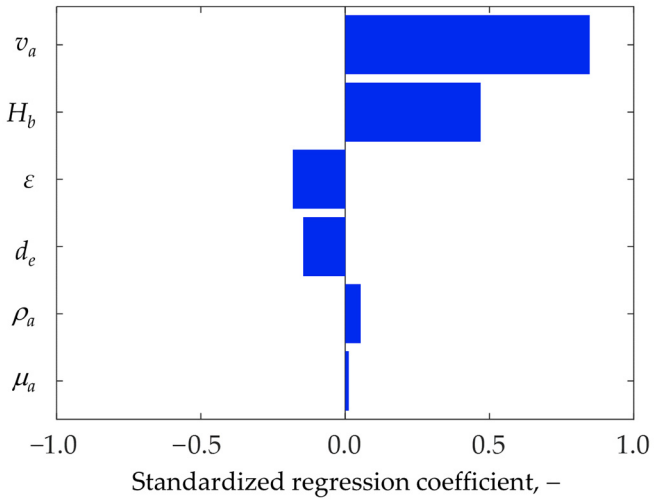

Figure 7. Standardized regression coefficients from sensitivity analysis including airflow velocity v_a, bulk depth H_b, pore volume ε, particle diameter d_e, air density ρ_a and dynamic air viscosity μ_a.

4. Conclusions

In this study, the resistance to airflow of a wheat grain bulk (*Triticum aestivum* L., cv. 'Pionier') under a set of air velocities, bulk depths and storage times was investigated. The physical characteristics of wheat kernels were experimentally assessed as a prerequisite for modeling the airflow resistance. For the characterization of ΔP vs. v_a relationship, the Matthies and Petersen model was employed, for which the product factor k was tailored for the specific wheat variety and experimental settings used in this study. From the fitting analysis, a goodness of fit with R^2 of 0.990, *RMSE* of 68.67 Pa and *MAPE* of 12.50% was observed for bulk depths ranging between 1.0 and 3.4 m and storage times between 1 and 236 h, which demonstrated a great potential of the employed model to describe the course of the experimental data with decent accuracy. Due to self-compaction, a spatial reduction of pore volume from 0.413 to 0.391 at bulk depths of 1.0 to 3.4 m after 1 h storage time and temporal reduction from 0.391 to 0.370 after 236 h storage time was observed, accordingly. Therefore, a disproportional increase of the pressure drop ΔP with bulk depth and storage time was observed, which was in contrast with the assumption of homogeneous and isotropic aerodynamic conditions in grain bulks often made in the literature. Thus, for practical application, higher power is required by the fan to maintain the required airflow velocity in bulk than when estimated from the default pore volume measured by the standard laboratory methods. The variation of pore volume ε was modeled and supported the development of a generalized model that could satisfactorily predict the airflow resistance of wheat bulk under self-compaction.

It could be shown that self-compaction plays a critical role in airflow resistance and therefore should be included in the design and analysis of cooling, aeration and low-temperature drying of in-store grain bulks. Further research should focus on the assessment of airflow resistances under self-compaction for other grains, moisture contents, bulk configurations and airflow velocity range. Moreover, the dynamics of grain compaction

until permanent equilibrium should be further investigated. In addition, advanced numerical methods should be employed for an in-depth analysis of kernel and bulk behavior subjected to a wide range of loads encountered in practice during the storage of grain bulks.

Author Contributions: Conceptualization, I.R., S.S., S.K. and J.M.; methodology, I.R., S.S., S.K. and J.M.; software, I.R.; validation, I.R.; formal analysis, I.R.; investigation, I.R.; resources, I.R. and J.M.; data curation, I.R.; writing—original draft preparation, I.R.; writing—review and editing, I.R., S.S., S.K. and J.M; visualization, I.R.; supervision, J.M.; project administration, I.R., S.S., S.K. and J.M.; funding acquisition, J.M. All authors have read and agreed to the published version of the manuscript.

Funding: This research was financially supported by the German Federal Ministry for Economic Affairs and Energy (BMWi)—Project number KF2607404LT4.

Institutional Review Board Statement: Not applicable.

Informed Consent Statement: Not applicable.

Data Availability Statement: Not applicable.

Acknowledgments: The authors are grateful to the technical team of the Institute of Agriculture Engineering for their assistance in the construction of components required for the experimental investigation. Special gratitude goes to Simon Munder and Sabine Nugent for their contributions to sensor development and language editing, respectively. Furthermore, authors are thankful to the editors and reviewers for their constructive comments, which helped to improve the quality and scientific substance of manuscript.

Conflicts of Interest: The authors declare no conflict of interest.

Nomenclature

a, c	Empirical constants, -
A	Kernel surface area, mm^2
d_a	Kernel arithmetic diameter, mm
d_e	Kernel equivalent diameter, mm
d_g	Kernel geometric diameter, mm
$d.b.$	Dry basis, -
f	Fan frequency, Hz
H_b	Grain bulk depth, mm
L	Kernel length, mm
k	Product factor, -
$\dot{m}$	Air mass flow rate, $kg \cdot h^{-1}$
m	Kernel unit mass, g
m_c	Aggregate mass of kernels in the container, g
m_{gr}	Mass of kernels soaked in toluene, g
$m_{fl,tol}$	Mass of pycnometer flask filled with toluene, g
$m_{gr,fl,tol}$	Mass of kernels, toluene solution and pycnometer flask, g
n	Number of observations, -
$MAPE$	Mean absolute percentage error, %
p	Probability level, -
Q	Air volume flow rate, $m^3 \cdot h^{-1}$
R^2	Coefficient of determination, -
R_a	Kernel aspect ratio, -
Re	Reynolds number, -
$RMSE$	Root mean square error, Pa
t	Elapsed storage time, h
T_a	Air temperature, °C
T	Kernel thickness, mm
v_a	Airflow velocity, $m \cdot s^{-1}$
V	Kernel unit volume, mm^3
V_b	Test bin volume, m^3
V_c	Container volume, m^3

V_p	Pycnometer volume, mm^3
W	Kernel width, mm
X	Moisture content, -
x,y	Independent and dependent variables in linear models, -
x_a	Air absolute humidity, g·kg^{-1}
Δx_a	Air saturation deficit, g·kg^{-1}
P	Pressure, Pa
ΔP	Pressure drop, Pa
ΔP_{obs}	Observed pressure drop, Pa
ΔP_{pred}	Predicted pressure drop, Pa
ε	Bulk pore volume, -
ε_0	Default pore volume, -
ε_{min}	Pore volume at the highest bulk depth, -
ζ	Friction factor, -
ϑ	Kernel sphericity, %
φ_a	Air relative humidity, %
ω	Fan rotational speed, min^{-1}
μ_a	Air dynamic viscosity, kg·m^{-1}·s^{-1}
ρ_a	Air density, kg·m^{-3}
ρ_b	Bulk density, kg·m^{-3}
ρ_{b0}	Default bulk density, kg·m^{-3}
ρ_s	Solid density, kg·m^{-3}
ρ_{tol}	Toluene density, kg·m^{-3}

Appendix A

Table A1. Variations of air conditions in the pore volume of the grain bulk during pressure drop experiments.

Storage Time t, h	Moisture Content X, kg·kg^{-1} d.b.	Temperature T, °C	Relative Humidity φ_a, %	Absolute Humidity x_a, g·kg^{-1}	Saturation Deficit Δx_a, g·kg^{-1}	Viscosity $\mu_a \times 10^{-5}$, kg·m^{-1}·s^{-1}	Density ρ_a, kg·m^{-3}
1	0.123 ± 0.001	17.18 ± 0.09	39.83 ± 0.69	4.84 ± 0.07	2.85 ± 0.04	1.80 ± 0.00	1.22 ± 0.00
65	-	15.02 ± 0.10	39.54 ± 0.19	4.23 ± 0.02	2.65 ± 0.04	1.79 ± 0.00	1.23 ± 0.00
164	-	16.30 ± 0.02	40.87 ± 0.02	4.70 ± 0.01	2.72 ± 0.00	1.80 ± 0.00	1.22 ± 0.00
236	0.122 ± 0.001	12.29 ± 0.02	34.04 ± 0.02	3.01 ± 0.01	2.66 ± 0.00	1.78 ± 0.00	1.24 ± 0.00

References

1. FAO. Food and Agriculture Data. Available online: http://www.fao.org/faostat/en/#data (accessed on 28 June 2022).
2. Awika, J.M. Major cereal grains production and use around the world. In *Advances in Cereal Science: Implications to Food Processing and Health Promotion*; ACS Publications: Washington, DC, USA, 2011; pp. 1–13.
3. Ziegler, V.; Paraginski, R.T.; Ferreira, C.D. Grain storage systems and effects of moisture, temperature and time on grain quality—A review. *J. Stored Prod. Res.* **2021**, *91*, 101770. [CrossRef]
4. Anukiruthika, T.; Jian, F.; Jayas, D.S. Movement and behavioral response of stored product insects under stored grain environments—A review. *J. Stored Prod. Res.* **2021**, *90*, 101752. [CrossRef]
5. Collins, D.A. A review on the factors affecting mite growth in stored grain commodities. *Exp. Appl. Acarol.* **2012**, *56*, 191–208. [CrossRef] [PubMed]
6. Mesterházy, Á.; Oláh, J.; Popp, J. Losses in the Grain Supply Chain: Causes and Solutions. *Sustainability* **2020**, *12*, 2342. [CrossRef]
7. Navarro, S.; Noyes, R.T. *The Mechanics and Physics of Modern Grain Aeration Management*; CRC Press: Boca Raton, FL, USA, 2001.
8. Labuza, T.P. Sorption phenomena in foods: Theoretical and practical aspects. In *Theory, Determination and Control of Physical Properties of Food Materials*; Springer: Berlin, Germany, 1975; pp. 197–219.
9. Lenovich, L.M. Survival and death of microorganisms as influenced by water activity. In *Water Activity: Theory and Applications to Food*, 1st ed.; Routledge: Oxfordshire, UK, 2017; pp. 119–136.
10. Chakraverty, A.; Singh, R.P. Grain storage. In *Postharvest Technology and Food Process Engineering*; CRC Press: Boca Raton, FL, USA, 2014; pp. 131–157.
11. Brooker, D.B.; Bakker-Arkema, F.W.; Hall, C.W. *Drying and Storage of Grains and Oilseeds*, 1st ed.; Springer Science & Business Media: New York, NY, USA, 1992.

12. Giner, S.A.; Denisienia, E. Pressure drop through wheat as affected by air velocity, moisture content and fines. *J. Agric. Eng. Res.* **1996**, *63*, 73–85. [CrossRef]
13. Kashaninejad, M.; Maghsoudlou, Y.; Khomeiri, M.; Tabil, L. Resistance to airflow through bulk pistachio nuts (Kalleghochi variety) as affected by moisture content, airflow rate, bed depth and fill method. *Powder Technol.* **2010**, *203*, 359–364. [CrossRef]
14. Olatunde, G.; Atungulu, G.G.; Sadaka, S. CFD modeling of air flow distribution in rice bin storage system with different grain mass configurations. *Biosyst. Eng.* **2016**, *151*, 286–297. [CrossRef]
15. Neethirajan, S.; Karunakaran, C.; Jayas, D.S.; White, N.D.G. X-ray Computed Tomography Image Analysis to explain the Airflow Resistance Differences in Grain Bulks. *Biosyst. Eng.* **2006**, *94*, 545–555. [CrossRef]
16. Alagusundaram, K.; Jayas, D. Airflow resistance of grains and oilseeds. *Postharvest News Inf.* **1990**, *1*, 279–283. [CrossRef]
17. Shedd, C.K. Resistance of grains and seeds to air flow. *Agric. Eng.* **1953**, *34*, 616–619.
18. Hukill, W.; Ives, N. Radial airflow resistance of grain. *Agric. Eng.* **1955**, *36*, 332–335.
19. Gunasekaran, S.; Jackson, C.Y. Resistance to airflow of grain sorghum. *Trans. ASAE* **1988**, *31*, 1237–1240. [CrossRef]
20. Nimkar, P.M.; Chattopadhyay, P.K. PH—Postharvest Technology: Airflow Resistance of Green Gram. *Biosyst. Eng.* **2002**, *82*, 407–414. [CrossRef]
21. Agullo, J.O.; Marenya, M.O. Airflow Resistance of Parchment Arabica Coffee. *Biosyst. Eng.* **2005**, *91*, 149–156. [CrossRef]
22. Hunter, A.J. Pressure difference across an aerated seed bulk for some common duct and store cross-sections. *J. Agric. Eng. Res.* **1983**, *28*, 437–450. [CrossRef]
23. Haque, E.; Ahmed, Y.N.; Deyoe, C.W. Static pressure drop in a fixed bed of grain as affected by grain moisture content. *Trans. ASAE* **1982**, *25*, 1095–1098. [CrossRef]
24. Ergun, S. Fluid Flow Through Packed Columns. *Chem. Eng. Prog.* **1952**, *48*, 89–94.
25. Carman, P.C. Fluid flow through granular beds. *Chem. Eng. Res. Des.* **1997**, *75*, S32–S48. [CrossRef]
26. Burke, S.P.; Plummer, W.B. Gas flow through packed columns. *Ind. Eng. Chem.* **1928**, *20*, 1196–1200. [CrossRef]
27. Patterson, R.J. *Airflow-Pressure Drop Characteristics of Packed Beds of Biological Particles*; Michigan State University: East Lansing, MI, USA, 1969.
28. Li, W.; Sokhansanj, S. Generalized equation for airflow resistance of bulk grains with variable density, moisture content and fines. *Dry. Technol.* **1994**, *12*, 649–667. [CrossRef]
29. Bern, C.J.; Charity, L.F. Airflow resistance characteristics of corn as influenced by bulk density. *ASAE Pap.* **1975**, *48*, 1137–1145.
30. Leva, M. *Fluidization*; McGraw-Hill: New York, NY, USA, 1959.
31. Matthies, H.J.; Petersen, H. New data for calculating the resistance to air flow of stored granular materials. *Trans. ASAE* **1974**, *17*, 1144–1149. [CrossRef]
32. Kumar, A.; Muir, W.E. Airflow resistance of wheat and barley affected by airflow direction, filling method and dockage. *Trans. ASAE* **1986**, *29*, 1423–1426. [CrossRef]
33. Turner, A.P.; Montross, M.D.; McNeill, S.G.; Sama, M.P.; Casada, M.C.; Boac, J.M.; Bhadra, R.E.; Maghirang, R.G.; Thompson, S.A. Modeling the compressibility behavior of hard red wheat varieties. *Trans. ASABE* **2016**, *59*, 1029–1038. [CrossRef]
34. Thompson, S.; McNeill, S.; Ross, I.; Bridges, T. Packing factors of whole grains in storage structures. *Appl. Eng. Agric.* **1987**, *3*, 215–221. [CrossRef]
35. Cheng, X.; Zhang, Q.; Yan, X.; Shi, C. Compressibility and equivalent bulk modulus of shelled corn. *Biosyst. Eng.* **2015**, *140*, 91–97. [CrossRef]
36. Rocha, J.C.d.; Pohndorf, R.S.; Meneghetti, V.L.; Oliveira, M.d.; Elias, M.C. Effects of mass compaction on airflow resistance through paddy rice grains. *Biosyst. Eng.* **2020**, *194*, 28–39. [CrossRef]
37. Molenda, M.; Montross, M.D.; McNeill, S.G.; Horabik, J. Airflow resistance of seeds at different bulk densities using Ergun's equation. *Trans. ASAE* **2005**, *48*, 1137–1145. [CrossRef]
38. Łukaszuk, J.; Molenda, M.; Horabik, J.; Szot, B.; Montross, M.D. Airflow resistance of wheat bedding as influenced by the filling method. *Res. Agric. Eng.* **2008**, *54*, 50. [CrossRef]
39. AOAC. *Official Methods of Analysis*, 16th ed.; Association of Analytical Chemist: Arlington, VA, USA, 1998.
40. Karaj, S.; Müller, J. Determination of physical, mechanical and chemical properties of seeds and kernels of *Jatropha curcas* L. *Ind. Crops Prod.* **2010**, *32*, 129–138. [CrossRef]
41. Sirisomboon, P.; Kitchaiya, P.; Pholpho, T.; Mahuttanyavanitch, W. Physical and mechanical properties of *Jatropha curcas* L. fruits, nuts and kernels. *Biosyst. Eng.* **2007**, *97*, 201–207. [CrossRef]
42. Mohsenin, N.N. *Physical Properties of Plant and Animal Materials*; Gordon & Breach Science Publishers Ltd.: Philadelphia, PA, USA, 1968.
43. ASAE. ASAE D272: Resistance to airflow of grains, seeds, other agricultural products, and perforated metal sheets. *Am. Soc. Agric. Biol. Eng.* **2003**, *3*, 569–576.
44. Miller, R.W. *Flow Measurement Engineering Handbook*, 3rd ed.; McGraw-Hill: New York, NY, USA, 1983.
45. Mühlbauer, W. *Handbuch der Getreidetrocknung: Grundlagen und Verfahren*; Agrimedia: Clenze, Germany, 2009.
46. Tabatabaeefar, A. Moisture-dependent physical properties of wheat. *Int. Agrophys.* **2003**, *17*, 207–211.
47. Karimi, M.; Kheiralipour, K.; Tabatabaeefar, A.; Khoubakht, G.; Naderi, M.; Heidarbeigi, K. The effect of moisture content on physical properties of wheat. *Pak. J. Nutr.* **2009**, *8*, 90–95. [CrossRef]

48. Molenda, M.; Horabik, J. Mechanical Properties of Granular Agro-Materials and Food Powders for Industrial Practice. In *Part I: Characterization of Mechanical Properties of Particulate Solids for Storage and Handling*; Institute of Agrophysics Polish Academy of Sciences: Lublin, Poland, 2005; p. 145.
49. Wang, D.; Dowell, F.E.; Lacey, R.E. Single wheat kernel size effects on near-infrared reflectance spectra and color classification. *Cereal Chem.* **1999**, *76*, 34–37. [CrossRef]
50. Nelson, S. Moisture-Dependent Kernel- and Bulk-Density Relationships for Wheat and Corn. *Trans. ASAE* **1980**, *23*, 139–0143. [CrossRef]
51. Petingco, M.C.; Casada, M.E.; Maghirang, R.G.; Thompson, S.A.; McNeill, S.G.; Montross, M.D.; Turner, A.P. Influence of kernel shape and size on the packing ratio and compressibility of hard red winter wheat. *Trans. ASABE* **2018**, *61*, 1437–1448. [CrossRef]
52. Markowski, M.; Żuk-Gołaszewska, K.; Kwiatkowski, D. Influence of variety on selected physical and mechanical properties of wheat. *Ind. Crops Prod.* **2013**, *47*, 113–117. [CrossRef]
53. Gürsoy, S.; Güzel, E. Determination of physical properties of some agricultural grains. *Res. J. Appl. Sci. Eng. Technol.* **2010**, *2*, 492–498.
54. Jayas, D.S.; Cenkowski, S. Grain Property Values and Their Measurement. In *Handbook of Industrial Drying*, 3rd ed.; CRC Press: Boca Raton, FL, USA, 2006.
55. Muir, W.; Sinha, R. Physical properties of cereal and oilseed cultivars grown in western Canada. *Can. Agric. Eng.* **1988**, *30*, 51–55.
56. Kraszewski, A.W. Wheat moisture content and bulk density determination by microwave parameters measurement. *Can. Agric. Eng.* **1992**, *34*, 327–335.
57. Petingco, M.C.; Casada, M.E.; Maghirang, R.G.; Thompson, S.A.; Turner, A.P.; McNeill, S.G.; Montross, M. Discrete Element Method Simulation of Wheat Bulk Density as Affected by Grain Drop Height and Kernel Size Distribution. *J. ASABE* **2022**, *65*, 555–566. [CrossRef]
58. Stephens, L.E.; Foster, G.H. Grain Bulk Properties as Affected by Mechanical Grain Spreaders. *Trans. ASAE* **1976**, *19*, 354–0358. [CrossRef]
59. White, F.M.; Majdalani, J. *Viscous Fluid Flow*, 2nd ed.; McGraw-Hill: New York, NY, USA, 2006.
60. Bakker-Arkema, F.W.; Patterson, R.J.; Bickert, W.G. Static pressure-airflow relationships in packed beds of granular biological materials such as cherry pits. *Trans. ASAE* **1969**, *12*, 134–0136. [CrossRef]
61. Cheng, X.; Zhang, Q.; Shi, C.; Yan, X. Model for the prediction of grain density and pressure distribution in hopper-bottom silos. *Biosyst. Eng.* **2017**, *163*, 159–166. [CrossRef]
62. Guillard, F.; Golshan, P.; Shen, L.; Valdes, J.R.; Einav, I. Dynamic patterns of compaction in brittle porous media. *Nat. Phys.* **2015**, *11*, 835–838. [CrossRef]
63. Grundas, S.; Szot, B.; Wozniak, W. Variability of the porosity of cereal grain layer under the influence of static loading. *Zesz. Probl. Postępów Nauk. Rol.* **1978**, *203*, 33–40.
64. Jayas, D.S.; Sokhansanj, S.; Moysey, E.B.; Barber, E.M. Airflow resistance of canola (rapeseed). *Trans. ASAE* **1987**, *30*, 1484–1488. [CrossRef]
65. Kay, R.L.; Bern, C.J.; Hurburgh, C.R., Jr. Horizontal and Vertical Airflow Resistance of Shelled Corn at Various Bulk Densities. *Trans. ASAE* **1989**, *32*, 733–0736. [CrossRef]
66. Siebenmorgen, T.J.; Jindal, V.K. Airflow resistance of rough rice as affected by moisture content, fines concentration and bulk density. *Trans. ASAE* **1987**, *30*, 1138–1143. [CrossRef]
67. Haque, E. Void fraction as a function of depth and pressure drops of packed beds of porous media formed by granular materials. *Trans. ASABE* **2011**, *54*, 2239–2243. [CrossRef]
68. Khatchatourian, O.A.; Savicki, D.L. Mathematical Modelling of Airflow in an Aerated Soya Bean Store under Non-uniform Conditions. *Biosyst. Eng.* **2004**, *88*, 201–211. [CrossRef]
69. Gao, M.; Cheng, X.; Du, X. Simulation of bulk density distribution of wheat in silos by finite element analysis. *J. Stored Prod. Res.* **2018**, *77*, 1–8. [CrossRef]